Metathesis-Enabled Formation of a Terminal Ruthenium Carbide Complex: A Computational Study

Corneliu Buda, Stephen R. Caskey, Marc J. A. Johnson*, and Barry D. Dunietz*

Chemistry Department, University of Michigan, 930 N. University, Ann Arbor, Michigan 48109

Received April 5, 2006

The energy profile of rare Ru carbide formation starting from an acetoxycarbene complex is studied using DFT methods. Three distinctive reaction pathways that differ in their initiation step are investigated. Two of the proposed reaction mechanisms have relatively similar activation barriers. Therefore, additional calculations have been performed using large size ligands (PCy_3), matching exactly the actual experimental system. In addition, the corresponding kinetic isotope effect has been evaluated and compared to the experimental measured value.

Introduction

Olefin metathesis has become a powerful tool for organic synthesis, following significant advances in catalyst design over the past 15 years.[1−6] Ru-based complexes in particular tolerate a wide variety of common functional groups.[1,2] Nevertheless, a few key functional groups are not tolerated in cross-metathesis (CM) reactions, but instead cause catalyst decomposition. In particular, given the importance of alkenyl halides as building blocks in transition-metal-catalyzed syntheses,[7] the general inability to synthesize alkenyl halides via CM is a long-standing limitation.[8*] [In contrast, there are a handful of recent examples describing ring-closing metathesis (RCM) involving α-halo-α,ω-dienes.[9] However, unlike cross-metathesis of alkenyl halides, which requires the formation of halocarbene intermediates that are very likely to be unstable, in these RCM reactions such intermediate halocarbene complexes are neither required nor implicated in the process.] Another process leading to limitation of metathesis catalysis is the formation of carbides from vinyl esters. In addition, carbide species have recently been found to play important roles as precursors to rapidly initiating olefin metathesis catalysts.[10]

Our recent studies[11] of metathesis reactions reveal the formation of a rare terminal carbide complex under some conditions. The carbide complex $Ru(C)(PCy_3)_2Cl_2$ (**a**)[10,12] was formed rapidly and quantitatively upon reaction of vinyl acetate with $Ru(CHPh)(PCy_3)_2Cl_2$ (**b**) in CH_2Cl_2.[11] As expected, the acetoxycarbene complex $Ru(CHO_2CMe)(PCy_3)_2Cl_2$ (**c**) was formed by metathesis with vinyl acetate, releasing styrene as the byproduct. However, intermediate **c** did not undergo further productive metathesis, but instead underwent rapid and quantitative conversion to **a**, concomitant with release of acetic acid.

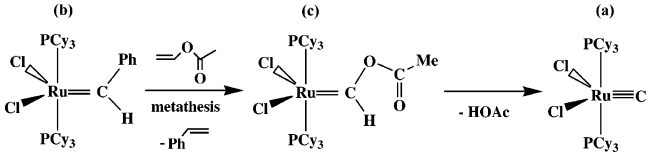

Vinyl carbonates similarly produce $Ru(C)(H_2IMes)(PCy_3)Cl_2$ [**d**; H_2IMes = 4,5-dihydro-1,3-bis(mesityl)imidazol-2-ylidene] from $Ru(CHPh)(H_2IMes)(PCy_3)Cl_2$ (**e**) in addition to effecting the conversion of **b** into **a**.[13] Furthermore as shown by Piers, these carbide complexes can be converted back into active metathesis catalysts in one step via rearrangement upon protonation with a suitable acid.[10] Moreover, a bridging carbide species is also a decomposition product of the RCM catalyst $Ru(CH_2)(H_2IMes)(PCy_3)Cl_2$.[14] These recent discoveries highlight the importance of carbide species to Ru-based olefin metathesis catalysis.

In this study, computational tools are used to study possible reaction mechanisms of the Ru carbide formation reaction. Three different mechanisms are considered. Two mechanisms involve the formation of a Ru chelating ring. These two pathways are suggested based on experimental observations of closely related compounds.[13,15] One of these pathways, which differ in their initiation steps, however, may be ruled out due to a prohibitively high reaction barrier. The third mechanism considers the possibility of a direct intraligand proton transfer. This mechanism involves a reaction coordinate where C−O bond cleavage is accompanied by a proton transfer, yielding the carbide moiety and acetic acid. This occurs without a change in the coordination number of the Ru center. The reaction barrier predicted for this

* To whom correspondence should be addressed. E-mail: mjaj@umich.edu; bdunietz@umich.edu.

(1) Grubbs, R. H. *Handbook of Metathesis*; Wiley-VCH: Weinheim, 2003.
(2) Trnka, T. M.; Grubbs, R. H. *Acc. Chem. Res.* **2001**, *34*, 18.
(3) Hoveyda, A. H.; Schrock, R. R. *Chem.--Eur. J.* **2001**, *7*, 945.
(4) Buchmeiser, M. R. *Chem. Rev.* **2000**, *100*, 1565.
(5) Fürstner, A. *Angew. Chem., Int. Ed.* **2000**, *39*, 3012.
(6) Schrock, R. R. *Tetrahedron* **1999**, *55*, 8141.
(7) Tsuji, J. *Transition Metal Reagents and Catalysts: Innovations in Organic Synthesis*; Wiley: New York, 2000; p 27.
(8) Morrill, C.; Grubbs, R. H. *J. Org. Chem.* **2003**, *68*, 6031.
(9) (a) Chao, W.; Meketa, M. L.; Weinreb, S. M. *Synthesis* **2004**, 2058. (b) Chao, W. C.; Weinreb, S. M. *Org. Lett.* **2003**, *5*, 2505. (c) Marhold, M.; Buer, A.; Hiemstra, H.; van Maarseveen, J. H.; Haufe, G. *Tetrahedron Lett.* **2004**, *45*, 57. (d) De Matteis, V.; van Delft, F. L.; de Gelder, R.; Tiebes, J.; Rutjes, F. *Tetrahedron Lett.* **2004**, *45*, 959. (e) Salim, S. S.; Bellingham, R. K.; Satcharoen, V.; Brown, R. C. D. *Org. Lett.* **2003**, *5*, 3403.
(10) Romero, P. E.; Piers, W. E.; McDonald, R. *Angew. Chem., Int. Ed.* **2004**, *43*, 6161.
(11) Caskey, S. R.; Stewart, M. H.; Kivela, J. E.; Sootsman, J. R.; Johnson, M. J. A.; Kampf, J. W. *J. Am. Chem. Soc.* **2005**, *127*, 16750.
(12) Carlson, R. G.; Gile, M. A.; Heppert, J. A.; Mason, M. H.; Powell, D. R.; Vander Velde, D.; Vilain, J. M. *J. Am. Chem. Soc.* **2002**, *124*, 1580.
(13) Caskey, S. R.; Ahn, Y. J.; Johnson, M. J. A.; Kampf, J. W. Manuscript in preparation.
(14) Hong, S. H.; Day, M. W.; Grubbs, R. H. *J. Am. Chem. Soc.* **2004**, *126*, 7414.
(15) Caskey, S. R.; Johnson, M. J. A.; Kampf, J. W. Manuscript in preparation.

10.1021/om0603060 CCC: $33.50
Publication on Web 08/29/2006

Scheme 1. Relative Energies (kcal mol^{-1}) Calculated for Reaction Path 1 Using B3LYP/LACVP**

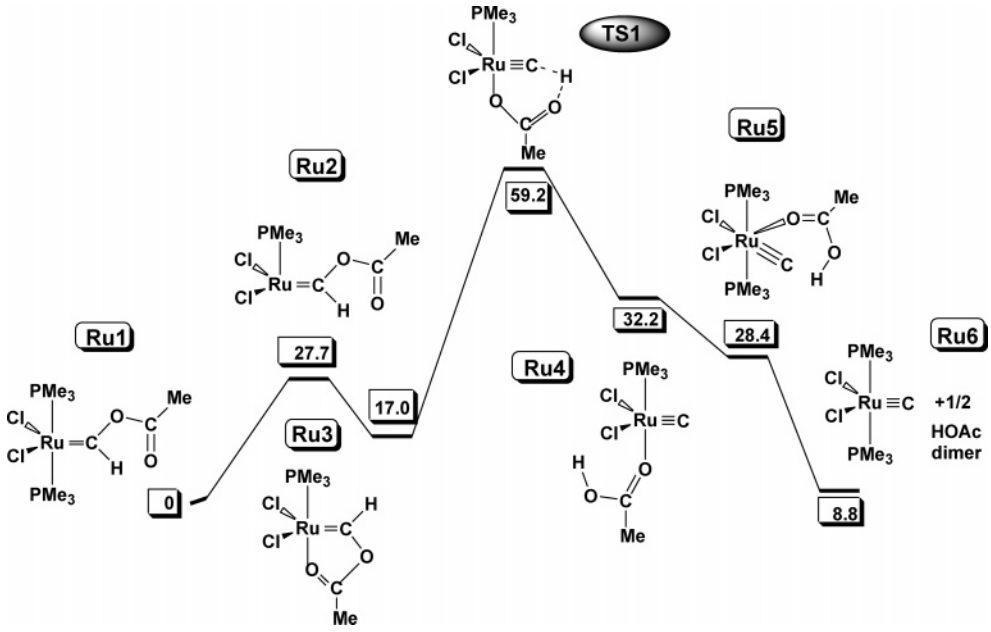

mechanism is comparable to the calculated activation barrier for the second mechanism considered. The different mechanisms are all compared below also by including solvation and entropy effects for the different intermediates and estimating their corresponding kinetic isotope effect (KIE) for comparison to available experimental data.

Computational Details

The different intermediates and transition states along the identified reaction pathways were obtained by geometry optimizations employing quantum mechanical methods. All models studied have neutral charge and a singlet spin state. The level of theory used is density functional theory with the widely used B3LYP functional[16] at the LACVP** basis set[17] level (the smaller LACVP and LACVP* sets were used to generate initial guesses). The Jaguar 5.5 package[18] was used to implement the calculations. All transition states were calculated without constraints and involve a single negative frequency associated with the reaction mode unless otherwise stated. Furthermore, all TS geometries were verified by optimization in backward and forward directions along the associated reaction coordinate to produce the relevant species. We have also incorporated solvation effects by employing the widely used continuum solvation model.[19]

Results and Discussion

The first step in the conversion of **b** into **a** (formation of compound **c**) involves double-bond metathesis; the mechanism of this transformation has been well studied both experimentally and computationally.[20,21] Accordingly, we concentrate on the second process, the conversion of **c** into **a**. Most of the calculations reported here concentrate on a model system. The model reaction investigated involves the transformation of an isolated Fischer carbene intermediate, $Ru(CHO_2CMe)(PMe_3)_2Cl_2$ (**Ru1**), into $Ru(C)(PMe_3)_2Cl_2$ (**Ru6**) and acetic acid (here Cy groups in **a** and **c** are modeled by Me groups as in **Ru1** and **Ru6**). Additional calculations where the actual reactant was studied have been employed as described below.

The Ru=C bond length in the optimized structure of the intermediate (**Ru1**) is 1.826 Å; the two substituents on the carbene are situated in the same plane as both Ru−P bonds. This agrees well with the structure of related $Ru(CHOEt)(PCy_3)_2Cl_2$,[22] except that the carbene fragment of the latter species lies approximately in the Cl−Ru−Cl plane, probably due to steric reasons. The ruthenium-containing product of the reaction closely resembles the reactant and differs mainly by replacing the Ru=C double bond with a Ru−carbide triple bond and having an acetic acid species released. The carbides **a** (and its model **Ru6**) and compound **c** (and its model **Ru1**) are best descried as (distorted) square pyramidal, diamagnetic, 16-electron complexes. The assignment of the configuration to square pyramid is based on the Verschoor[23] definition for distinguishing between square pyramid and trigonal bypyramid configurations. In this procedure a geometric parameter is obtained from the difference of the two largest angles defined by Ru ligands. A value of 0.0 corresponds to a square pyramid and 1.0 corresponds to a pure trigonal bipyramidal structure. For the complexes considered here, this geometric parameter is found to be 0.40 and 0.39 for **Ru1** and **Ru6**, respectively, which are closer to the square pyramid limit. The calculated length of the Ru−carbide bond is 1.655 Å, which compares well to that of **a**.[24]

Several possible reaction paths have been investigated. The first two pathways examined involve the formation of a five-

(16) (a) Becke, A. D. *J. Chem. Phys.* **1993**, *98*, 5648. (b) Vosko, S. H.; Wilk, L.; Nusair, M. *Can. J. Phys.* **1980**, *58*, 1200. (c) Lee, C.; Yang, W.; Parr, R. G. *Phys. Rev. B* **1988**, *37*, 785.
(17) Hay, P. J.; Wadt, W. R. *J. Chem. Phys.* **1985,** *82***,** 299.
(18) *Jaguar 5.5*; Schrodinger, L.L.C.: Portland, OR, 2003.
(19) Tannor, D. J.; Marten, B.; Murphy, R.; Friesner, R. A.; Sitkoff, D.; Nicholls, A.; Ringnalda, M.; Goddard, W. A., III; Honig, B. *J. Am. Chem. Soc.* **1994**, *116*, 11875.
(20) Sanford, M. S.; Love, J. A.; Grubbs, R. H. *J. Am. Chem. Soc.* **2001**, *123*, 6543.
(21) (a) Cavallo, L. *J. Am. Chem. Soc.* **2002**, *124*, 8965. (b) Fomine, S.; Vargas, S. M.; Tlenkopatchev, M. A. *Organometallics* **2003**, *22*, 93. (c) Suresh, C. H.; Baik, M. *Dalton Trans.* **2005**, 2982. (d) Suresh, C. H.; Koga, N. *Organometallics* **2004**, *23*, 76. (e) Bernardi, F.; Bottoni, A.; Miscione, G. P. *Organometallics* **1998**, *17*, 16. (f) Vyboishchikov, S. F.; Bühl, M.; Thiel, W. *Chem.--Eur. J.* **2002**, *8*, 3962. (g) Costabile, C.; Cavallo, L. *J.* Am. Chem. Soc. **2004**, *126*, 9592.
(22) Louie, J.; Grubbs, R. H. *Organometallics* **2002**, *21*, 2153.
(23) Addison, A. W.; Rao, T. N.; Reedijk, J.; van Rijn, J.; Verschoor, G. C. *J. Chem. Soc., Dalton Trans.* **1984**, 1349.
(24) Hejl, A.; Trnka, T. M.; Day, M. W.; Grubbs, R. H. *Chem. Commun.* **2002**, 2524.

Scheme 2. Relative Energies (kcal mol^{-1}) Calculated for Reaction Path 1a

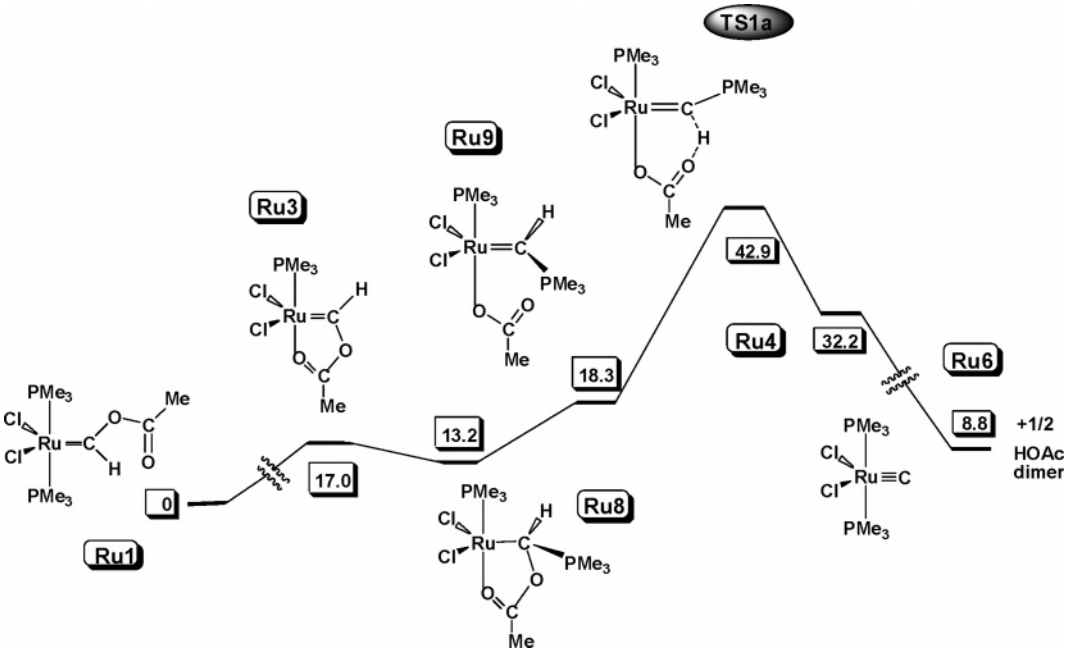

membered chelating ring with the Ru atom. These reaction pathways differ in the initiation step. In Scheme 1, the Ru atom is activated by dissociation of a PMe_3 ligand and is followed by rebinding this group in a subsequent step. This may be supported by the observation of small amounts of free PCy_3 and $Ru(CHOAc)(PCy_3)Cl_2$ in the reaction mixtures at partial conversion of **c** to **a**.

This first considered reaction mechanism involves the endothermic dissociation of a phosphine ligand generating **Ru2**, as illustrated in Scheme 1. Experimental evidence relating to the phosphine dissociation barrier in a closely related complex has been reported. In particular, the dissociative exchange of PCy_3 from **b** is found to have an activation barrier of 23.6 ± 0.5 kcal mol^{-1} at 25 °C in toluene-d_8.[20] The energy of the resulting species, intermediate **Ru2** and free PMe_3, is 27.7 kcal mol^{-1} above **Ru1**. In **Ru2**, the carbene α-H atom and the OAc group are still in the same plane and the Ru−P and Ru−C bond lengths remain almost unchanged (2.243 and 1.817 Å, respectively). An isomer of **Ru2** was obtained by switching the sites occupied by the H atom and OAc group; this corresponds to 180° rotation about the Ru═C bond. This **Ru2′** species was found to be only 0.5 kcal mol^{-1} less stable than **Ru2**.

The phosphine dissociation leads to a reactive four-coordinate 14-electron species, which corresponds to the intermediate that is required for olefin metathesis. Interestingly, excess vinyl acetate does not appear to undergo metathesis in the presence of **c**; instead, the stable carbide **a** is formed. The low coordination number and electron density at the Ru atom underlie the formation of the chelating ring, where the carbonyl O atom serves as a donor to the electrophilic Ru center. This process is exothermic, generating the intermediate **Ru3**, which is more stable than **Ru2** by almost 11 kcal mol^{-1}. The phosphine dissociation barrier is partially compensated by this spontaneous ring formation reaction. Intermediate **Ru3** is a 16-electron species involving a five-atom chelate ring configuration with a long donor−acceptor O−Ru bond of 2.253 Å. The Ru−C distance in **Ru3** is only slightly decreased to 1.811 Å from 1.817 Å in **Ru2**.

From this point, the reaction path in Scheme 1 continues with formation of the ruthenium−carbide triple bond in **Ru4** via a proton transfer step leading to the cleavage of the ring's C−O bond. In this scheme, **TS1** denotes the transition state for this step. In **Ru4**, the newly formed HOAc molecule is coordinated to the Ru atom through the carbonyl oxygen atom. This intermediate is slightly stabilized by rebinding a phosphine ligand, forming **Ru5**; in this structure, the HOAc ligand moves into a site *cis* to both PMe_3 ligands. Dissociation of the HOAc ligand follows, yielding the final carbide product, **Ru6**. All the steps following the formation of **TS1** are exothermic.

In this scheme, **TS1** is the transition state defining the reaction barrier. In **TS1**, the Ru−O bond length is reduced to 2.096 Å from 2.253 Å in **Ru3**. The Ru−O bond is changing from a donor−acceptor type to a covalent bond. In addition, the incipient Ru−carbide bond in **TS1** is significantly shortened (1.669 Å) and closely approaches that found in the product, **Ru6**. **TS1** is characterized by a bridging H atom, which is shared by both carbon and oxygen atoms as illustrated (at 1.134 Å distance from the C and 1.650 Å from O; the Ru−C−H angle is 139.0°). The structure of **TS1** is very similar to that of $Ru(C\text{-}p\text{-}C_6H_4Me)(PCy_3)I_3$, which is a stable, isolable species.[15]

The vibrational mode of **TS1** that corresponds to the reaction coordinate involves the H atom oscillating between the C and O atoms. The H atom is transferred to O and the OAc group migrates toward the Cl−Ru−O plane, resulting in the **Ru4** configuration. This step introduces a 42 kcal mol^{-1} energy barrier, which is higher than the barriers found for the alternative reaction mechanisms investigated (see below). Furthermore, the activation energy predicted for this mechanism is about 60 kcal mol^{-1}. Therefore, this pathway is ruled out.

An alternate progression of the mechanism illustrated in Scheme 1 starting from the **Ru3** intermediate was considered as well. In this scenario, illustrated in Scheme 2, a free phosphine ligand binds directly to the C atom bonded to the Ru center, generating **Ru8**. The phosphine group in **Ru8** is oriented perpendicular to the plane of the five-atom ring. This species is more stable than **Ru3** by only 3.8 kcal mol^{-1}. This phosphine orientation facilitates the dissociation of the C−O bond, producing **Ru9**. Here both H and PMe_3 groups are situated in the Cl−Ru−Cl plane. The following transition state in this mechanism is denoted as **TS1a**.

Scheme 3. Relative Energies (kcal mol^{-1}) Calculated for Reaction Path 2

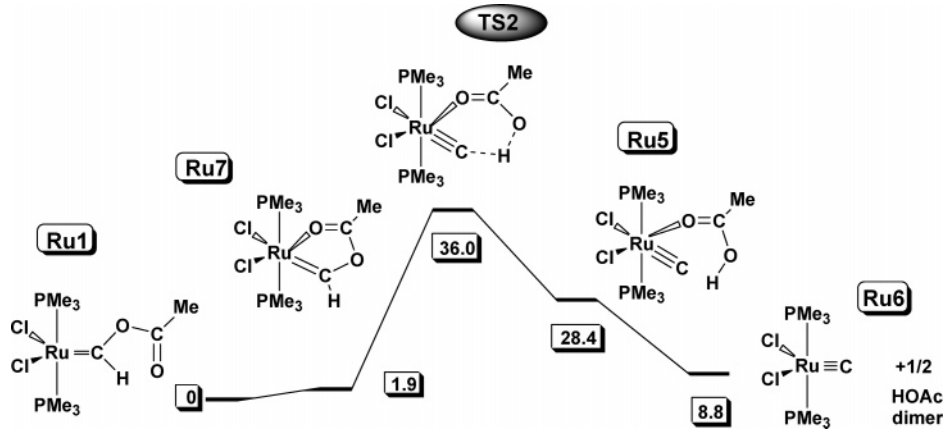

TS1a involves the migration of H from the C toward the O atom. This vibrational motion is associated with a single imaginary frequency of 570.3 cm^{-1}. The H atom is located at 1.471 Å from the C and 1.150 Å from the O. The **TS1a** atomic configuration differs from **TS1** by the presence of the phosphine group linked to the C atom. It features a more extended C−H bond and a much reduced reaction barrier with about 16 kcal mol^{-1} energy reduction. The formation of **Ru4** follows by relaxation of the H atom toward the oxygen and by rotation of the carboxylic group toward the plane defined by the Ru and Cl atoms. **Ru4** is the same as the intermediate following **TS1** in Scheme 1. We note that while the activation energy of **TS1a** is lower than **TS1**, other reaction mechanisms described below, however, exhibit even lower activation barriers.

The other reaction paths considered in this work are not activated through a removal (and then rebinding) of a phosphine group, despite the observation that small quantities of free PCy_3 and $Ru(CHO_2CMe)(PCy_3)Cl_2$ (represented by model species **Ru2**) exist in equilibrium with **c** in the actual system.[13] Although both experiment and calculations permit the formation of species such as **Ru2**, these are not productive intermediates on the direct pathway linking **Ru1** to **Ru6**, but are formed in a side equilibrium with **Ru1**. In addition, our observation that a closely related compound, $Ru(CHO_2COEt)(PCy_3)_2Cl_2$, undergoes conversion to **a** in the solid state[13] further indicates a mechanism that does not involve phosphine dissociation. Therefore, the actual mechanism may not involve any dissociation of PCy_3 ligands. Instead, the alternative reaction path involves a less complex mechanism of proton transfer.

In the second considered path, illustrated in Scheme 3, the reactant is activated following an increase in the coordination number of Ru. In this scheme, the activation is achieved by coordination of the carbonyl O atom to the Ru center, resulting in a six-coordinate intermediate, **Ru7**. This intermediate contains a five-membered chelate ring that lies in the Cl−Ru−Cl plane. **Ru7**, the new intermediate, which has an 18-electron configuration, is found to be very close in energy to **Ru1** (only 1.9 kcal mol^{-1} higher in energy). The O−Ru bond length in **Ru7** is 2.213 Å, consistent with donor−acceptor character, whereas the Ru═C bond length is 1.842 Å, only marginally longer than the 1.826 Å value of **Ru1**. This mechanism is calculated to have a lower activation barrier, as indicated in Scheme 3 and discussed next.

The reaction path 2 continues by transforming **Ru7** to the identical six-coordinate intermediate as in Scheme 1, **Ru5**. This transformation involves a proton transfer within the ring similar to that in Scheme 1. However, in this reaction mechanism the Ru atom maintains a high coordination number with an 18-electron configuration in its transition state, which leads to a relatively lower lying transition state, **TS2**.

This transition state is illustrated in Figure 1. In **TS2**, the H atom undergoing transfer is shared by both O and C atoms (selected bond lengths and angles: O−H 1.348 Å, C−H 1.246 Å, Ru−C 1.693 Å, Ru−C−H angle 127.5°). The Ru−C−H angle is less than 180°, while the C atom hybridization is intermediate between sp and sp^2. A single imaginary frequency has been identified with the value of 952.6 cm^{-1}. As illustrated, this vibration mode is associated with the oscillation of the indicated H atom between the C atom of the incipient carbide ligand and the O atom of the OAc group.

The calculated activation energy is about 36 kcal mol^{-1}, compared to 60 or 42 kcal mol^{-1} calculated in Schemes 1 and 2. The lack of phosphine dissociation along this pathway implies that the conversion of **c** to **a** should be unaffected by added phosphine. Experimentally, we find that conversion of **5** into **1** is independent of PCy_3 concentration,[13] an observation that by itself rules out the mechanism of Scheme 1, but is consistent with those in Schemes 3 and 4 (see below for details of the latter). The reaction continues from **TS2** to form **Ru5**, where the carbide ligand is formed by completion of the H migration to the O atom. Dissociation of the acetic acid ligand leads to the final product **Ru6** as with Scheme 1.

Next, an additional mechanism that lacks the dissociation of the phosphine group is investigated. In this mechanism, which is found to possess energetics similar to that in Scheme 3, a proton transfer within the C−OAc (OAc = O-acetyl) ligand is involved. In this mechanism, the Ru center remains five-coordinate at all times, undergoing neither dissociation nor association of a ligand. Scheme 4 illustrates this reaction mechanism, which involves a single step along a complex reaction coordinate. This reaction coordinate first involves the activation of the C−O ester bond. In the identified TS (**TS3**),

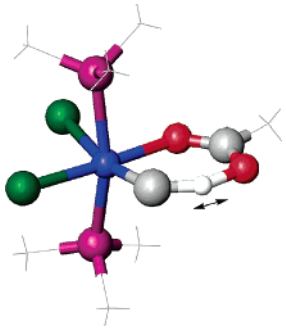

Figure 1. Transition state geometry for reaction path 2.

Scheme 4. Relative Energies (kcal mol^{-1}) Calculated for Reaction Path 3[a]

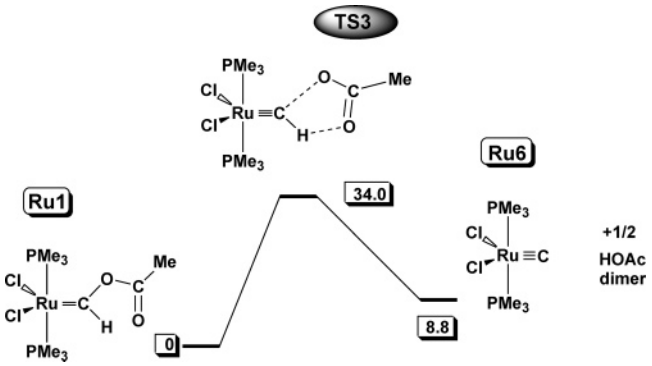

[a] A similar scheme has been also calculated with a larger model including PCy_3 ligands, with about 0.5 kcal/mol reduction of the energy barrier.

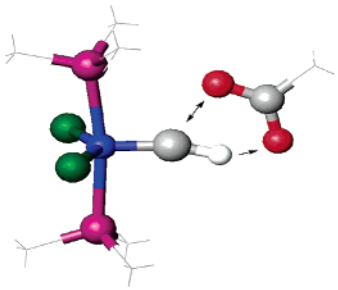

Figure 2. The calculated **TS3** involves the hydrogen-bonded complex. The arrows indicate the major displacement of atoms along the reaction coordinate.

the C−O bond is elongated at 2.139 Å versus the 1.372 Å bond length in the reactant. In **TS3** the C−H bond length is only slightly increased to 1.190 Å from the stable 1.094 Å bond length in the reactant. The measured H−O distance in **TS3** is 1.472 Å. In addition, the Ru═C bond length in **TS3** is considerably shortened from 1.826 Å in Ru1 to 1.702 Å, which is almost three-quarters of the way to the carbide bond length in the product **Ru6** (1.655 Å).

The reaction coordinate then proceeds via a direct proton transfer within the ligating Fischer carbene moiety from the ligating C atom to the terminal O atom.

The calculated **TS3** geometry is illustrated in Figure 2, where the atoms that define the reaction coordinate with their movement are highlighted by arrows. The activation energy corresponding to this scheme is 34 kcal mol^{-1}. It is important, however, to note that this calculated **TS3** involves two imaginary frequencies. The first frequency at 474 cm^{-1} is the recognized reaction coordinate described above. The additional very flat frequency (at only 8.5 cm^{-1}) is found to be associated with the tendency of the OAc moiety to be shifted away from the P−Ru−P plane. Our attempts to eliminate this frequency upon further optimization of **TS3** have all failed. We ascribe this to a combination of numerical instabilities and model truncation associated with long-range intramolecular dispersion forces.

Therefore we have employed calculations involving nontruncated models where PCy_3 is used instead of PMe_3. The use of the bulkier ligand leads to a more realistic orientation of the HOAc group and therefore to the cleanup of the spurious imaginary frequency. The resulting geometry indeed involves a single imaginary frequency at 352.6 cm^{-1}, which corresponds to the mode described above for **TS3**. This structure also was

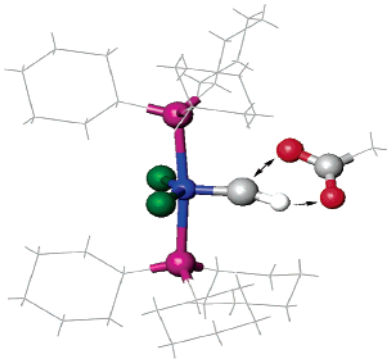

Figure 3. The calculated geometry for **TS3** using PCy_3 ligands. Note the shift of the carboxyl plane away from the plane defined by the P−Ru−P atoms.

Table 1. KIE, C−H Bond Variations, and Energy Barriers for Different Reaction Mechanisms[a]

			activation energy (kcal mol^{-1})		Gibbs (kcal mol^{-1})
TS model	KIE	Δ_{C-H} (Å)	w/o solvent	with solvent	with solvent
TS1	nc	0.040	59.2 (−3.9)	54.8 (−4.2)	34.8
TS1a	3.1	0.377	42.9 (−2.7)	35.0 (−2.1)	33.4
TS2	2.9	0.152	36.0 (−2.9)	33.2 (−3.3)	27.7
TS3	2.4	0.096	34.0 (−2.7)	34.5 (−2.6)	30.9

[a] nc = not calculated; (ZPE) values relative to reactant.

confirmed to lead to the reactant and products by following geometry optimizations in the forward and backward directions of the reaction coordinate.

The presence of the bulkier PCy_3 groups has caused the plane of the chelate ring to shift away from the P−Ru−P plane. The smaller model calculation placed the ring in the same plane as the P−Ru−P plane. However, with the larger model, the tilt angle of the ring is found to be close to 45° relative to the P−Ru−P plane. All other geometrical features (i.e., the bond lengths) reported above for **TS3** remain almost unaltered. The structure of the **TS3** with the larger model is depicted in Figure 3.

The calculated activation energy using this larger model is slightly reduced to 33.5 kcal mol^{-1}. This is only a 0.5 kcal mol^{-1} difference from the results involving the smaller models. We note that all our attempts to calculate **TS2** with the larger model have failed. The geometries of **TS2** and **TS3** differ by the position and number of atoms involved in the chelate ring. In **TS2** one O atom from the carbonyl group is linked to the Ru center, generating a six-atom ring, while in **TS3** the Ru center is not incorporated in the ring. We suggest that the additional intramolecular repulsions due to the bulkier ligands do not allow the O atom to bind to the Ru center, making the **TS2** geometry less feasible. This leads us to suggest that the presence of the bulkier ligands (PCy_3) may favor the **TS3** instead of **TS2** geometry.

To further analyze the different mechanisms, we have also modeled the solvation effect. The continuum solvent model,[19] despite its coarse representation, is found to perform quite well for similar species.[25] The solvent (CH_2Cl_2), as shown in the Table 1, lowers the energetical barrier for all mechanisms. The activation energies of the considered mechanisms with the solvent effect included are also shown to be relatively similar to each other. Activation barriers between 33 and 35 kcal mol^{-1} are now predicted for mechanisms 2, 3, and 1a. However,

(25) Benitez, D.; Goddard, W. A., III. *J. Am. Chem. Soc.* **2005**, *127*, 12218.

it is possible that models employing several explicit solvent molecules located strategically within the first solvation shell would provide an even better description of the solvent effect and allow a better discrimination of a specific mechanism. It is also important to note that with solvent effect included all geometries including the transition states show additional imaginary frequencies. The vibration modes corresponding to these new frequencies are associated with rotation of the methyl groups or other motions irrelevant to the reaction coordinate.[26] We estimate that fully optimized geometries with the solvent would decrease the energy by 2−3 kcal mol^{-1} for all species. Therefore, these spurious frequencies have a limited to no effect on the calculated activation barrier. In the table we also include the correction for the energy barriers by including the zero-point energy (ZPE) due to the molecular vibrations. We find that the ZPE further lowers the barriers by about 3 kcal mol^{-1} for the different considered routes. The ZPE correction values are provided in parentheses.

The effect of entropy is also considered. The Gibbs free energy values for the transition states relative to the reactant are provided in Table 1. We find that the entropy effect for mechanisms 3 and 1a is minimal. However, the effect on mechanism 2 is to further reduce the barrier by an additional 2 kcal mol^{-1}. This allows mechanism 2 to have the lowest reaction barrier, one that is only 7 kcal mol^{-1} above the measured experimental value. The most dramatic entropy effect is found with mechanism 1; however, the final barrier for this mechanism is still substantially the highest of all considered reaction routes.

In the overall chemical process studied, the final carbide product is obtained free of acetic acid. Therefore, the final energetic comparison of the product must include the equivalent dimerization energy of the acetic acid. This dimerization involves strong double hydrogen bonding and is calculated to be 20.4 kcal mol^{-1} at the LACVP** basis set. Thus, the overall reaction is calculated to be slightly endothermic with 8.8 kcal mol^{-1}, but is entropically favored. The overall reaction barrier due to Gibbs free energy is slightly exothermic, with a −2.7 kcal mol^{-1} difference when the solvent effect is included. This is in close agreement with our experimental measurements.

As a final point, we have also evaluated the kinetic isotope effect (KIE) values for the reaction schemes described above and contrast them to the experimentally measured value. The KIE values are calculated using frequencies of the reactant and the three most stable transition states obtained by replacing the hydrogen with a deuterium atom. The formal expression is provided elsewhere.[27] We have also corrected all calculated frequencies by using the empirical scaling factor of 0.96.[28] The KIE values were calculated at standard temperature (298 K). The variation of the C−H bond length and the activation energies from the reactant to the transition states are also listed in Table 1.

The smallest calculated KIE value of 2.4 corresponds to the mechanism illustrated in Scheme 4. This is the closest to the experimentally determined value of 1.5 measured in dichloromethane solution.[13] This also corresponds with the lowest change in the C−H bond length and the smallest activation electronic energy. The other two calculated KIE values, 2.9 for **TS2** and 3.1 for **TS1a**, follow the same trends relative to bond variations and energy barriers. Therefore, the reaction mechanism illustrated in Scheme 4 features the best agreement with available experimental data of all mechanisms considered in this study with respect to the isotope effect.

The calculated mechanisms predict activation energies that are less than 10 kcal mol^{-1} above the experimental value of $\Delta G^{\ddagger} = 20.6$ kcal mol^{-1} for the spontaneous conversion of **c** into **a**, with concomitant release of $MeCO_2H$.[13] We note, in addition, that experimentally, solvent effects are known to be strong: the $\Delta H^{\ddagger}$ value quoted above pertains to the reaction in dichloromethane, which is complete within 20 min at 25 °C. In contrast, in benzene the intermediate **c** is sufficiently long-lived to be isolable in pure form. Future computational studies of this system may require explicit solvent models to properly represent the important effect of the solvent on the reaction mechanism.

We have also considered additional variants of the above mechanism. In these alternative routes, two of the ligands are allowed to switch their positions on the Ru center. In this switch, a Cl and a PMe_3 ligand exchange their positions on the Ru center during the reaction coordinate. This has the effect of generating isomers in which the two chloride ligands are *cis* rather than *trans*. *Cis*−*trans* isomerism of this type is important in some closely related systems that undergo olefin metathesis.[25,29] This aspect was considered for all the above mechanisms. This leads to more polarized versions of the different TSs and intermediates. The energies of the corresponding isomers have been calculated for all intermediates and transition states in the gas phase and in the solvent. We find as expected that these alternative species have a higher gas phase potential energy surface and possess stronger stabilization due to the solvation effect than the original configurations. However, in the balance of these two contradicting effects we find that all of the alternative mechanisms feature higher reaction barriers even when entropy is considered as well. Therefore, we conclude that it is unlikely for these ligands to switch their locations during the reaction.

In conclusion, computational methods have been successfully used to determine the more favorable reaction pathways. The first considered mechanism is defined through related experimental observations. However it was found to involve less favorable energetics than other alternatives. The two alternative mechanisms are found to possess comparable energetics when employing truncated models. In one mechanism (Scheme 3), the rate-determining step involves a proton transfer step within a chelating organic ring. In the alternate mechanism (Scheme 4) the activation step involves a direct proton transfer from the ligating C to the O within the Fischer carbene ligand. This is coupled with cleavage of the C−O ester bond. This mechanism is also confirmed by results from using untruncated models. In addition, we note that the reaction mechanisms provide quite similar agreement with the available experimental data with respect to activation barriers and the KIE values. Additional experimental and computational work may be required to further analyze this complex system.

In future work, we will also address the high stability of the terminal carbide **Ru6**, focusing on analyzing the nature of the

(26) Bailey, B. C.; Fan, H.; Huffman, J. C.; Baik, M.-H., Mindiola, D. J. *J. Am. Chem. Soc.* **2006**, *128*, 6798.
(27) Abu-Hasanayn, F.; Goldman, A. S.; Krogh-Jespersen, K. *J. Phys. Chem.* **1993**, *97*, 5890.
(28) Rauhut, G.; Pulay, P. *J. Phys. Chem.* **1995**, *99*, 3093.
(29) (a) Ung, T.; Hejl, A.; Grubbs, R. H.; Schrodi, Y. *Organometallics* **2004**, *23*, 5399. (b) Seiders, T. J.; Ward, D. W.; Grubbs, R. H. *Org. Lett.* **2001**, *3*, 3225.

carbide bond. This may lead to procedures to interfere with the Ru−C bond stability by manipulating the Ru fragment to achieve a less stable carbide species. A more reactive carbide bond is expected to be highly useful in bond-forming reactions.

Acknowledgment. We would like to acknowledge the financial and technical support received from University of Michigan for the duration of this research.

OM0603060